Arabian Journal of Geosciences (2018) 11: 129
https://doi.org/10.1007/s12517-018-3462-1

ORIGINAL PAPER

Ground calcium carbonate (GCC) from the Barre de Ghomrassene in Southeast Tunisia: a suitable raw material for paint industry

Tahar Aloui[1] · Ikram Jabli[1] · Arwa Hermassi[1] · Fredj Chaabani[1]

Received: 2 October 2017 / Accepted: 2 March 2018 / Published online: 22 March 2018

Abstract

The main scope of the present work is to investigate the potential of using ground calcium carbonate (GCC) from the Barre de Ghomrassene (BDG) in Southeast Tunisia in paint industry. In order to evaluate the performance of the material and the formulated paint films, representative raw specimens of main deposits of naturel GCCs in the Mediterranean basin and Middle East countries such as extra-white limestone from the Abiod Formation (Feriana region in West-Central Tunisia), Aşıgediği Formation (Niğde Group, South Central Turkey), and Samalut Formation (Elminea, South Cairo, Egypt) were considered. Samples were ground to specific surface of about 3000 cm^2/g and were subjected to detailed characterization including chemical and mineral composition, physical, and chromaticity characteristics. Results show that the GCC from the lower part of the Barre de Ghomrassene is, in most, dark and grainstone in texture, which limit its use in paint and coating application. Elsewhere, it is marked by high purity degree (generally more than 97% calcite); high lightness (more than 86.5, 95.2 in average) with relatively low chromaticity ($a^* < 3.3$, $b^* < 9.1$); low oil intake (17.4 g/100 GCC); very low electrolyte levels; good pH buffering (close to 9); accepted ranges of density and abrasion (2.65–2.7 and 10–18, respectively); good grindability; low levels of harmful components such as MgO, SiO_2, Fe_2O_3, and acid insoluble residue (less than 0.1% each); and improved rheological properties. The BDG seems to be a suitable filler for paint when mixed with water, styrene acrylic, and common additives. The formulated paint films meet all standard requirements, in that they have very good opacity, matt visual dualgloss 20/60°, high luminescence ($L^* = 96.4$), suitable hardness (145 s), good adhesion (B5), and sufficient impact resistance (1.5 kg m). The performances of these films are analogous to those based on Abiod and Samalut formations (natural carbonate), but they are slightly less lighter than those based on Aşıgediği Formation (metamorphic carbonate). Hence, the studied GCC can be used to substitute them in particular for local GCCs from the Abiod Formation, which are limited and over exploited.

Keywords Barre de Ghomrassene · Abiod Formation · Aşıgediği Formation · Samalut Formation · White limestone · GCC · Paint and coating · Filler · Material characterization and valorization

Introduction

Limestone, or calcium carbonate, represents about 10% of sedimentary rocks. White calcium carbonate is rare and comprises only less than 4% of the earth crust. High-grade calcium carbonate (extra-white calcium carbonate or industrial limestone) is even rarer. Major dark substances that alter its whiteness are iron and manganese oxides, organic matter, and pyrite. Lighter silicates that give a white powder upon grinding such as muscovite (white mica) are generally not harmful (Pohl 2011). Most of the large deposits of limestone are located in China, Vietnam, and India.

High-grade ground carbonate fillers are micronized carbonates with a high whiteness. Suitable Mediterranean deposits include Cretaceous chalk (France), marine limestones (Spain, Italy, Tunisia, Germany, Greece, Egypt), and calcite marbles (Italy, Turkey, Greece). The calcite marbles reach the highest degrees of whiteness (Pohl 2011).

From geologic point of view, calcium carbonate outcrops are frequent in Tunisia. Substantial reserves are in Jurassic (Barre de Ghomrassene Member) and Cretaceous (Bouhedma, Orbata, and Zebbag formations and equivalents), but most of them are

✉ Tahar Aloui
tahar.aloui@edunet.tn; aloui.t@laposte.net; aloui.t10@gmail.com

[1] Laboratory of Geosciences, Mineral Resources, Energy and the Environment, Department of Geology, Faculty of Sciences of Tunis, University of Tunis El Manar, Campus, 2092 Tunis, Tunisia

totally to partially dolomitzed, which limit their potential use. Extra-white limestone is very limited and localized. The main known deposits are in Abiod Formation (Aloui and Chaabani 2007, 2008), Merfeg Formation, and to a lesser extent Early Eocene Nummulitic limestone of El Garia Formation. But the most suited are those of Abiod Formation at the Feriana Mountain (Aloui et al. 2017).

The white limestone is used as paving, curb, tile, slab, cladding, and sculpture. In mineral industries, it is employed as ground calcium carbonate (GCC) and precipitated calcium carbonate (PCC) in white cement, glass, paint and paper industries (Aloui and Chaabani 2007, 2008; Aloui et al. 2017), lime metallurgical flux, water treatment (Sdiri and Bouazir 2014), sugar refining, mineral fillers, agriculture, animal feed, calcium chemicals, flue-gas desulfurization (FGD), plastics, and polyvinyl chloride pipes. The suitability of use for any given application depends in particular, but not only, on mean particle size and distribution, color, chemical composition, and mineral purity of the material (Cox et al. 1977; Broad et al. 1993).

In the paint industry, GCC is the most broadly used of the extender pigments. It is employed as a bright, yet inexpensive extender for titanium dioxide to increase the bulk and lower the cost, as well as to control rheology and gloss levels of the end product (Broad et al. 1993; Aas 1996). In matt emulsions, up to 30% by weight of the paint is limestone. GCC is used throughout the range of water- and solvent-based coatings for both interior and exterior applications (Dillon et al. 2014). In exterior application, calcite has good weather ability except in highly acidic atmospheres. Its hydrophilic nature accounts for easy dispersibility, especially in water-based systems. Recently, some outcrops of extra-white limestone were reported for the first time in the Barre de Ghomrassene towards the south of Tataouine.

The present work attempts to investigate the potential of using ground calcium carbonate (GCC) from the Barre de Ghomrassene (BDG) in paint industry. This may promote the sustainable development in the region and preserve the limestone of the Abiod at Feriana Mountain, which are extensively exploited, for more value applications.

Geological settings

The area under investigation is located between the latitude 33° 18″ to 32° 37′ 42″ and longitude 10° 18′ 30″ to 10° 31′ 22″ (Fig. 1). The outcrops range from Permian to Quaternary in age. The Barre de Ghomrassene unite (Callovian p.p. to Early Oxfordian?, Enay et al. 2002) was defined for the first time by Busson (1967) as Member of Foum Tataouine Group (or simply the Tataouine Formation). It forms a beige to white limestone bar of 18 to 25 m thick that weakly deeps towards the west. This bar is well exposed in the landscape as a remarkable cliff, which can be traced over 200 km from Beni Kheddache to Dehibat to the south. The barre starts with bioturbated oolithic limestone (grainstone), with bioclastic debris and small granules (barrier bank, Fig. 2e), overlain by irregular-bedded limestone (packstone to mudstone), containing abundant fauna of foraminifera, nautilus, echinoderms, tabulate coral (Fig. 2g), polyps in living position (Fig. 2h), brain coral (Fig. 2i), lamellibranches (Fig. 2f) and brachiopods: *Terebratula* (Fig. 2j), and ends fining upward by white to beige coral and well-developed sponge bioherm limestone (Fig. 2a, b). Bioherms may reach 6 m high and up to 32 m width at Zaafrane Wadi (Ben Ismail et al. 1989). Laterally, these bioherms pass into thin bedded limestones. Towards the south of Tataouine City, the limestone becomes soft, finer and whiter, while the fauna becomes very sparse and small in size. The topmost beds may display flint nodules.

Methods and techniques

Sampling and origin of raw materials

Fifty samples of limestone from the Barre de Ghomrassene were collected (Fig. 1). The sampling through the whole lithology depended on homogeneity and thickness. If the unit thickness was less than 2 m, one sample was taken from its middle. If the unit thickness exceeded this limit, one sample was taken every 2 m.

In addition to white limestone from the Barre de Ghomrassene (Tataouine region in Southeast Tunisia) and the Abiod Formation (Feriana region in West-Central Tunisia; M'Rabet 1987; Aloui and Chaabani 2006, 2007, 2008), samples from Aşıgediği Formation (Niğde Group, South Central Turkey) and Samalut Formation (Elminea area, South Cairo, Egypt) were considered. These deposits represent the main sources of naturel ground calcium carbonate in the Mediterranean basin as in the Middle East countries.

The Niğde massif is composed essentially of metamorphic rocks that form the Niğde Group. According to their lithological characteristics they are differentiated and described as Gümüşler, Kaleboynu, and Aşıgediği formations and Üçkapılı granodiorite (Göncüoğlu 1977). The Aşıgediği Formation, from which samples were collected, represents the stratigraphically youngest outcrops of this Group and is composed largely of monomineralic calcite marble with interlayered quartzite and amphibolite (Whitney and Dilek 1998; Whitney et al. 2003).

The Samalut Formation (Middle Eocene) was introduced by Bishay (1961) at Samalut City on the right bank of the Nile River near the el-Teir Hill. The Samalut Formation is 90–110 m thick and composed mainly of shallow marine reefal carbonate (nummulitic limestones), with few white, fine limestone intercalations. It shows

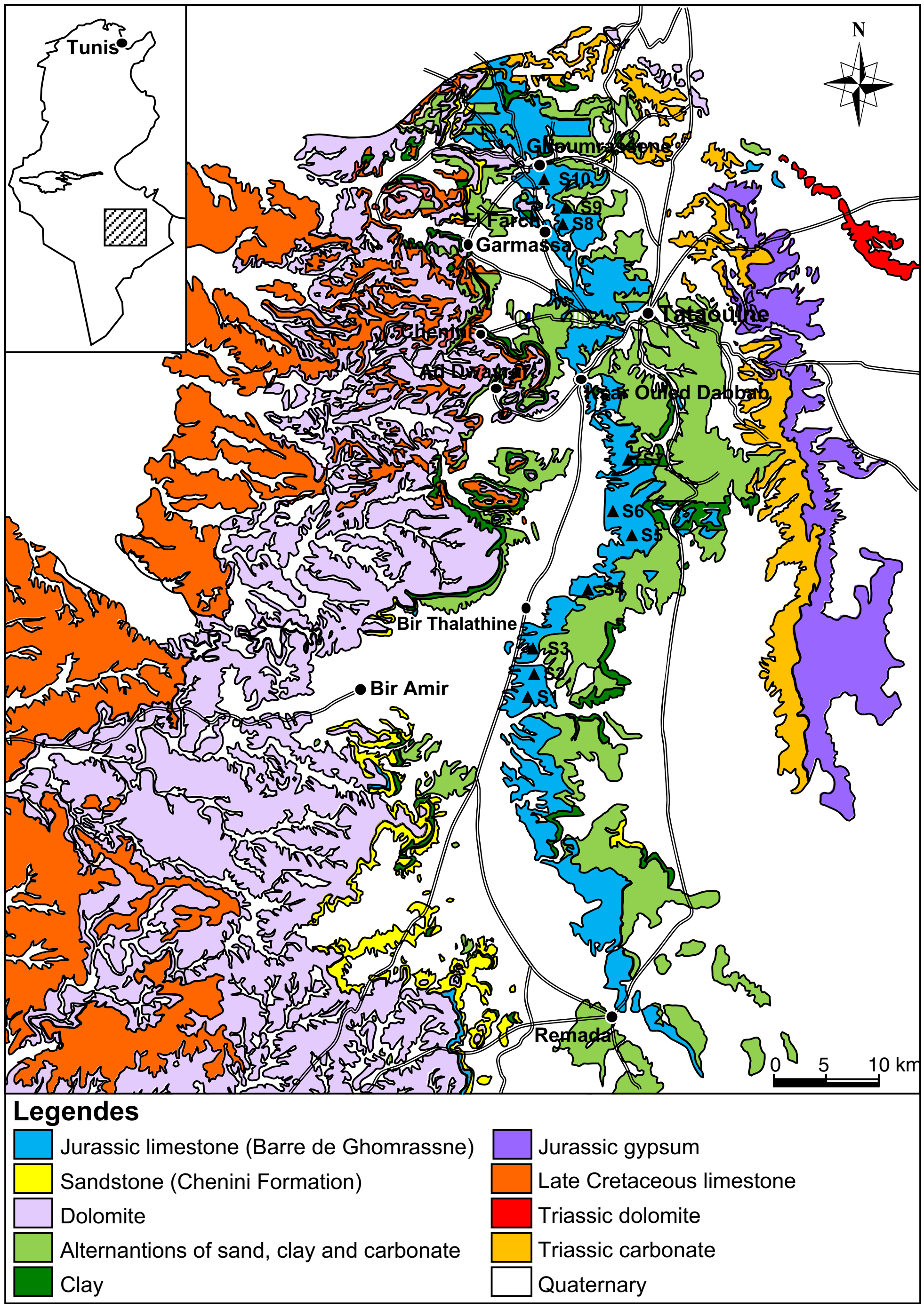

Fig. 1 Geological map of the study area showing le extend of the Barre de Ghomrassene and sampling site S1 to S10 (modified after the Geological Map of Tunisia, scale *1/500000*)

scattered flint nodules at the base and hard dolomitic laminated limestone at the top (Bishay 1966).

Preparation of samples

The grinding stage of GCC materials is an increasingly important process in wide application in a large number of industries including cement, paint, coating, lacquer, rubber, ceramic, and ink. This can be attributed to factors such as enhancement of the physico-chemical performance of the end product with decreased particle size such as optical properties, reaction kinetics, packing characteristics, and strength (Somasundaran 1978; Conley 1983). The reduction of particle size is very expensive and the energy requirements as well as cost per tone of filler (Eswaraiah et al. 2015). Hence, the grindability may be a decisive factor in selecting raw materials (Ariffin 2003).

The grinding time affects full particle size distribution (PSD), and hence Blaine surface area and whiteness of GCCs (Bentz et al. 1999). In paint industry, PSD is one

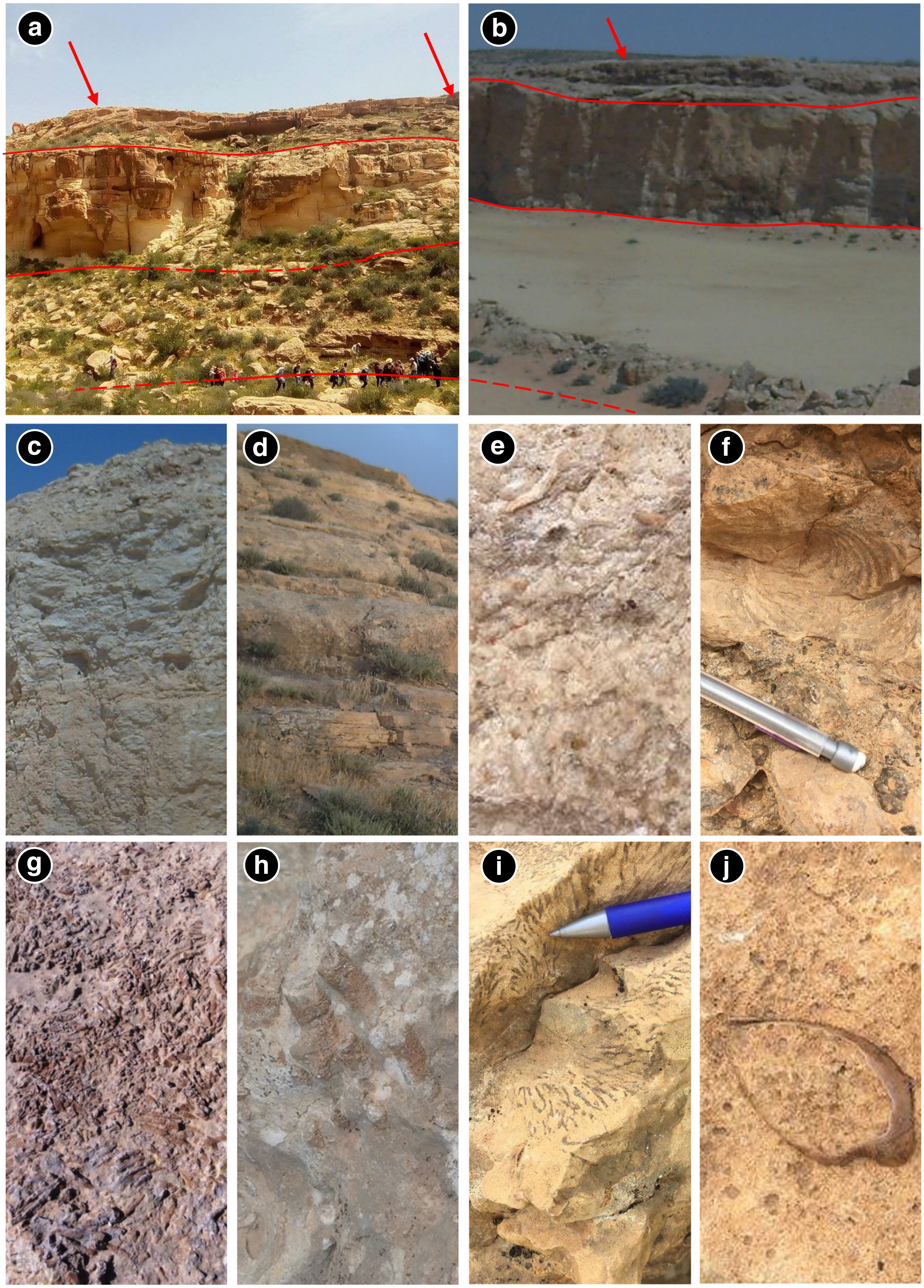

Fig. 2 Outcrops of the Barre de Ghomrassene Member. **a** At Wadi El Khil (20 km NW Tataouine) showing the three terms of the Barre de Ghomrassene. **b** Near Bir Thalathine village (30 Km SW of Tataouine). **c** Closer view of **b**. **d** At El Farech City (3 km NW of Tataouine). **e** Oolithes (barrier bank environment, active agitation condition). **f** Lamellibranche. **g** Tabulate coral (*Syringopora*?). **h** Polyps in living position. **i** Brain coral. **j** Brachiopods (*Terebratula*, open-sea condition). The tip of the arrow points to the bioherm constructions

of the most critical of physical properties of fillers and pigments (Karakaş and Celik 2012), because it controls the appearance of the end product and promotes rapid chemical reactions, through the exposure of large surface areas to reactants (binder and additives). The full particle size distribution is difficult to apply in correlation with other parameters with accuracy or to describe the fully PSD even for the same material and under similar conditions of grinding process (Klieger 1994). Allen (1990), demonstrated that the specific surface, and hence the grinding time, controls in great part the particle size distribution and shape in many mineral industries such as cement and paint production. The particle size distributions are given as grading zone, in which lower, upper, and middle limits of PSDs are identified. This is particular interesting when valorizing many raw materials.

In the laboratory, all samples were systematically washed by compressed air to remove clays and fines and dried in an oven at a temperature of about 105 °C for 1 h. The limestone samples were ground using HERZOG high-speed mill (HSM). In order to facilitate the grinding of the limestone and avoid the sticking of the material, a few drops of ethanol were added as a grinding aid (6 drops in average). The high-speed of the drive motor enables the grinding of even hard materials with short process time and good reproducibility. The optical properties and full grain size distribution were then determined after each 1 min until whiteness became constant and 100% of particles were lower than 45 μm. The PSD that falls at the middle of grading zone was considered as representative sample to study its suitability for paint use if needed.

Titanium dioxide (TiO_2) is the most important white pigment widely used in paint industry because it efficiently scatters visible light, thereby imparting the appearance of the film in term of whiteness, brightness, glossiness, and opacity when incorporated into a coating. Typical properties of a commercial TiO_2 pigment used in the present work are given in Table 1 according to the manufacturer's datasheet. Likewise, three local commercial water borne paints were arbitrarily provided, which will serve as typical end product to assess the performance of the elaborated paint based on the GCC from the Barre de Ghomrassene.

Chemical composition

The contents of alumina oxide (Al_2O_3), calcium oxide (CaO), chrome oxide (Cr_2O_3), phosphorus pentoxide (P_2O_5), ferric oxide (Fe_2O_3), magnesium oxide (MgO), dimanganese trioxide (Mn_2O_3), titan dioxide (TiO_2), and silicon dioxide (SiO_2) from the raw material were determined by X-ray fluorescence (XRF) analysis on a Philips PW 1606 spectrometer (France) with automated sample feed, reverse potential end window with rhodium anode and operated at 50 kV, 40 mA. Beads were prepared by fusing mixtures of 0.7 g of powdered sample with 6 g of lithium tetraborate (LiB_4O_7) (Ruste 1978; Blanco-Varela et al. 1997).

Table 1 Typical properties of TiO_2

Specification	Value
TiO_2 (%)	96
Specific gravity (g/cm^3)	4.2
Bulk specific gravity (kg/m^3)	700
Brightness L*	98
Red-green reading (a*)	2.3
Yellow-blue reading (b*)	2.1
Refractive index	2.7
Oil absorption (ml/100 g TiO_2)	19
pH	7.5
Specific resistance (kohm.cm)	8
Average particle size (μm)	0.25

These steps taken in preparation of the sample led to a more homogeneous material and, consequently, had the advantage of obtaining a more accurate XRF analysis. The contents of potassium oxide (K_2O) and sodium oxide (Na_2O) were obtained by atomic absorption spectrophotometry. The determination of the content of sulfur trioxide (SO_3) was carried out by a gravimetric technique.

Acid insoluble residue

The acid insoluble residue (IR) was used to determine the noncarbonate fraction present in the GCC samples. A portion of the GCC sample was weighed and cautiously dispersed, with agitation, into 10% hydrochloric acid solution. The mixture was left to react at ambient temperature until no further reaction took place and then filtered under vacuum through a pre-weighed Gelman DM-450 membrane filter. The later was allowed to dry to constant weight under ambient room conditions. The amount of acid insoluble residue was then calculated as the following:

$$\mathrm{IR}(\%) = \frac{\text{Weight of residue}}{\text{Weight of GCC sample}} \times 100$$

pH measurements

A 5-g GCC was dispersed in 50 ml of distilled water. The pH value was measured at room temperature using a pH meter. The pH electrode was calibrated against the buffer solution with a fresh calibration solution of pH 7.

Mineral composition

X-ray diffraction (XRD) analyses were carried out using a Philips PANalytical X'Pert PRO X-ray diffractometer with an automatic divergence slit, a spinner, an X'celator, and CuKa radiation at a scan speed of 0.01° 2θ/s. The acceleration power applied was 40 kV, with a current of 40 mA. Data were evaluated by the X'pert HightScoreplus ® program.

Optical properties

Optical performance is an important specification of fillers for many applications such paint and white cement. All samples were dried systematically and analyzed for color using pressed tablets according to the International Commission on Illumination CIE 1976 $L^*a^*b^*$ color system (CIE 1986). Here, the color measurement is based on three distinct stimuli: L^* indicates the factor of luminescence or brightness (white-black reading), a^* (red-green reading), and b^* (blue-yellow reading). The CIE $L^*a^*b^*$ color space was chosen since it is widely used in paint and coating industry.

Grainsize distribution

The particle size distribution (PSD) of GCC plays a key role during the production processes (calcium absorption and retention) as well as in quality control of painted film. The particle size distribution data include mean and median sizes of the tested GCCs, their 45-µm percent passing value, size, and spread factors (n, X_0) of the Rosin–Rammler distribution and Blaine specific surface area values. The grainsize distribution of the GCC (0.01–2100 µm) was performed using a laser particle sizer Analysette 22/NanoTec made by FRITSCH GmbH (Germany). The 3th and 97th percentiles were employed to appreciate the fine and coarse particles in the GCC distribution respectively. Likewise, the percentages of material below 3 µm and above 15 µm were used as indicators for the finer and coarser grades, respectively.

Thermal behavior

To detect volatiles and organic matter and to evaluate how materials exhibit either mass loss or gain during the decomposition and oxidation process, samples were tested for simultaneous differential thermal analysis (DTA) and thermal gravimetric analysis (TGA) under normal atmosphere using a Labsys device. The TGA data were collected at a rate of 20 °C/min to a final temperature of 1050 °C.

Mechanical behavior of the raw material

Density

A dry, weighed glass pycnometer (M_p), was filled with distilled water and then weighed (M_{p+w}), giving the weight of water ($M_w = M_{p+w} - M_p$). The GCC powder was added to the pycnometer (M_p), which is then weighed (M_{p+GCC}). The weight of the powder is $M_{GCC} = M_{p+GCC} - M_p$. The pycnometer is then filled with distilled water, in which the GCC sample was completely insoluble. The weight of water and GCC sample is M_{w+GCC}, and thence the density of the powder d_{GCC} was calculated as following: $d_{GCC} = M_{GCC}/(M_w - M_{w+GCC})$. The test was done at room temperature and pressure as suggested by the ASTM D854 norm (ASTM 2014a).

Abrasion test

The appreciation of toughness and abrasion characteristics of limestone aggregates was done using Micro-Deval testing in accordance with ASTM D 6928 norm (ASTM 2017a). A high-quality aggregate must be able to stand up to the wear and tear of the manufacturing process and the effects of transportation and repeated stockpiling of the end product (Köhler et al. 2012).

Oil absorption

The oil absorption is the amount of refined linseed oil, by either weight or volume, necessary to produce a firm, smooth and cohesive paste from 100 g of dry pigment (GCC). The oil consumption is used to give an indication of the effect of different pigments on the flow properties of the system and to calculate the pigment loading limits (Köhler et al. 2012). The oil adsorption was done according to ASTM D 281 norm (ASTM 2016).

Production of paint

Formulation of paint

A paint is composed of pigments, solvents, resins (binders), and additives. The pigments give the paint film color and enhance coating. Resins help it dry and form the paint film. Solvents give the paint the correct consistency to make it easier for application. Additives, however, were added in small quantities to give new performance to the film such as fillers, antifungicidal agents, driers, and pH adjuster. All these additives were selected and optimized according to their compatibility in particular with the styrene acrylic binder in terms of polarity (Karakaş and Celik 2012). The objective of this formulation was to elaborate wall paints for interior use that prevent algae and microbial growth, washable and odorless with very good adhesion properties. The interior paints are mainly concerned with esthetic characteristics such as color and gloss, rather than protection, which are relatively easy to apply (Koleske 2012).

Seventy percent by weight of GCC was mixed with 30% of water, resin, and pigments to form a high concentrated millbase. The millbase was dispersed using 12 mm ceramic ball mill on a magnetic stirrer at 1000 rpm for 4 h. This step aims to grind the calcite particles, making them smaller and dispersing them throughout the mixture. After that, the mixture was screened using a 63-μm sieve. The millbase was diluted and mixed with further classic resin, solvent, and additives (Table 2), to give it the desired properties with particular viscosity, flexibility, and drying rate. The formulated paint was inspected for its viscosity, color, pH, density, fineness of grind, and dispersion. The pigment volume concentration (PVC) was kept constant because it determines the structure of the film, which may cause dramatically influence paint properties (Chaudhury and Pocius 2002; Gündüz 2015).

Viscosity of paint

The viscosity or consistency is the measure of resistance of paint to constant flow. It is determined according to the ASTM D562–10 (2014b) norm using a Krebs viscometer. The rotational speed was maintained constant at 200 rpm. As the rheology is temperature sensitive, the viscosity was determined at ambient temperature of 25 °C. Results were reported in Krebs units (KU).

Physical and mechanical properties of the paint films

The elaborated paint films were checked for several tests including color, luminescence, glossiness, drying time, dry film thickness, hardness, impact resistance, and adhesion.

Visual glossiness

Gloss (sheen) is an aspect of the visual perception of the film and, considering the psychological impact of painted products on a consumer, is as important as the color itself. Gloss is measured by quantifying the reflectance of a known amount of light from a painted film surface. It was measured at dualgloss 20/60° following the ASTM D523 norm (ASTM 2008).

Wet film thickness

The measurement of wet film thickness provides an early appreciation about the coating application process and the spreading rate of paints (Köhler et al. 2012). It was carried out on a rigid substrate in compliance with requirements of the ASTM D1212 norm (ASTM 2013).

Table 2 Average composition of formulated paint

Material	Quantity (%)	Role
Biocide	0.4	Prevents the attack on paint by microorganisms
Anti-bacterial	0.26	
PU[a] thickening agent	0.1	Controls the rheological properties of paints
HEC[b] thickening agent	0.26	
GCC (filler), $d = 1.7$	61	Provides volume solids at a low cost, whiting pigment and reduces the shrinkage which occurs during curing
Pigment (TiO_2), $d = 4.2$	5.7	Improves the whiteness
Water, $d = 1$	23.35	
Dispersant agent	0.006	Prevents sedimentation particularly of high-density pigments
Wetting agent	0.1	Aids wetting of the pigments by the binders and prevents flocculation of the pigment particles, leads to the formation of a uniform, haze-free color and a uniformly high luster of the film
Defoamer	0.2	Prevents foaming during paint manufacture and application and promotes release of air from the coating film during drying
Binder (styrene acrylic), $d = 1.2$	6	Improves physical properties of film such as elasticity, hardness, adhesion to the substrate, appearance, impact deformation, chemical resistance, and resistance to weathering
pH adjuster	0.02	
Coalescing agent	0.6	Aids film formation, particularly at lower temperatures; improves leveling, gloss, adhesion, and scrub resistance
Blistering agent	0.004	Prevents formation of bubbles or pimples on the painted surface caused by moisture in the wood by painting before the previous coat has dried thoroughly or by excessive heat or grease under the paint
Total	100	

[a] Polyurethane

[b] Hydroxyethyl cellulose

Dry through time

The film was not distorted or detached when the thumb was applied to it in a specified manner and rotated through 90°. It was carried out at ambient temperature on a clean glass substrate and under no direct sunlight.

Hardness

The coating hardness was determined by pendulum damping test (König or a Persoz pendulum hardness tester) with the time, in seconds, noted for the swing amplitude of the pendulum to decrease by a specified degree when set into oscillation on the dried film as specified by the ISO 1522 norm (ISO 2006).

Impact resistance

The impact resistance test was carried out following the ASTM D2794 norm (ASTM 2010). It was done by placing a flat cured coated panel under a weighted spherical ball assembly and then dropping the weighted ball (1.7 kg) on the panel from different heights (max 1 m). The impact resistance was determined based on the displacement of the cylinder in which the ball was mounted.

Adhesion

The adhesion of cured painted films was appreciated using a cross-hatch test because it is the suitable method for films thinner than125 μm (Köhler et al. 2012). Given the dry thickness range of elaborated films (80–130 μm), a cross-cut of 1.9 cm with 6 cuts spaced 2 mm apart was used. The results were interpreted according to the scale specified in the ASTM D3359 norm (ASTM 2017b).

Data analysis

With a view to determine the relative contribution of the chemical (CaO, SiO_2, Al_2O_3, Fe_2O_3, Na_2O, K_2O, MgO, SO_3, Sr, TiO_2, and LOI) and optical (L^*, a^*, b^*) variables in the entire data set multivariate ordination techniques, as the principal components analysis (PCA) and the agglomerative hierarchic clustering (AHC) techniques, were performed using XLStat-pro software (Addinsoft 1995–2017, Ver 19.4).

All original chemical and optical variables were assumed to have an equal importance in their influence on material quality. The implementation and running of PC and AHC were described in detail in our previous works (Aloui and Chaabani 2008; Aloui et al. 2012).

Results and discussions

Chemical and mineral properties of the Barre de Ghomrassene carbonate

The CaO content varied from 52.9 to 55.34% with an average of 54.4% (Table 3). Top values were observed near the Khechem el Miit area and seemed to decrease gradually north towards the El Farech village (Fig. 1). Compared with the pure calcite (CaO, CO_2), limestones from the BDG Member are characterized by a high to very high degree of purity (Cox et al. 1977), which grades from 94.5 at S10 to 98.6% at S5 (97.1% on average at zero loss on ignition). The extremely low content of MgO (less than 0.4% on average), indicates a weak dolomitization process

Table 3 Average chemical composition of the BDG and standard ranges of major and minor element oxides analyzed by XRF method

	CaO	MgO	SiO_2	Fe_2O_3	Al_2O_3	MnO	Na_2O	K_2O	P_2O_5	SO_3	Cr_2O_3	TiO_2	Sr	Cl	LOI
Typical[a]	> 54.3	< 3	< 2	< 1	< 3	< 0.1	< 0.1	< 0.1	< 0.1	< 0.3	<0.1	–	–	–	> 42.7
S1	54.46	0.26	0.81	0.33	0.18	0.008	0.01	0.07	0.012	nd	nd	0.01	0.014	0.032	43.72
S2	53.96	0.37	0.8	0.49	0.25	0.009	0.02	0.11	0.012	nd	nd	0.01	0.012	0.118	43.68
S3	53.94	0.29	0.87	0.53	0.24	0.009	0.01	0.09	0.012	nd	nd	0.01	0.012	0.020	43.82
S4	55.15	0.26	0.43	0.39	0.13	0.008	0.01	0.07	0.008	nd	nd	0.01	0.012	0.011	43.51
S5	55.24	0.2	0.29	0.15	0.08	0.009	0.01	nd	0.032	nd	nd	nd	0.010	0.034	43.75
S6	54.73	0.27	0.48	0.21	0.12	0.033	0.01	nd	0.016	nd	nd	nd	0.013	0.027	43.99
S7	53.95	0.34	0.77	0.34	0.16	0.008	0.01	0.08	0.011	nd	nd	0.01	0.013	0.018	43.84
S8	54.85	0.27	0.4	0.2	0.11	0.007	0.01	nd	0.010	nd	nd	nd	0.012	0.019	43.89
S9	54.68	0.26	0.64	0.13	0.1	0.005	0.01	nd	0.008	nd	nd	nd	0.011	0.017	43.85
S10	52.9	1.5	0.73	0.89	0.07	0.024	0.02	nd	0.015	nd	nd	0.01	0.009	0.027	43.8

nd not detected, (−) no common specification is furnished

[a] Köhler et al. 2012

Table 4 Correlation matrix of Pearson (n) of chemical and optical parameters

Variables	CaO	SiO_2	Al_2O_3	Fe_2O_3	MgO	K_2O	Na_2O	TiO_2	MnO	P_2O_5	Sr	Cl	LOI	L^*	a^*	b^*
CaO	*1*															
SiO_2	*− 0.91*	*1*														
Al_2O_3	*− 0.9*	*0.99*	*1*													
Fe_2O_3	*− 0.81*	*0.88*	*0.9*	*1*												
MgO	*− 0.89*	*0.68*	*0.65*	0.54	*1*											
K_2O	*− 0.74*	*0.84*	*0.87*	*0.97*	0.42	*1*										
Na_2O	*− 0.89*	*0.97*	*0.98*	*0.93*	0.62	*0.92*	*1*									
TiO_2	*− 0.9*	*0.99*	*0.99*	*0.89*	*0.66*	*0.85*	*0.98*	*1*								
MnO	0.14	− 0.11	− 0.12	− 0.3	− 0.12	− 0.34	− 0.18	− 0.14	*1*							
P_2O_5	0	0.14	0.14	− 0.04	− 0.03	0	0.06	0.16	0.28	*1*						
Sr	*− 0.87*	*0.98*	*0.97*	*0.8*	*0.65*	*0.75*	*0.94*	*0.98*	− 0.06	0.13	*1*					
Cl	− 0.09	0.13	0.18	0.38	− 0.11	0.47	0.21	0.12	− 0.1	0	− 0.02	*1*				
LOI	*0.98*	*− 0.94*	*− 0.92*	*− 0.82*	*− 0.87*	*− 0.75*	*− 0.9*	*− 0.93*	0.21	− 0.04	*− 0.9*	− 0.11	*1*			
L^*	*0.99*	*− 0.92*	*− 0.9*	*− 0.8*	*− 0.89*	*− 0.73*	*− 0.9*	*− 0.91*	0.14	− 0.01	*− 0.9*	0	*0.97*	*1*		
a^*	*− 0.93*	*0.92*	*0.93*	*0.93*	*0.72*	*0.88*	*0.95*	*0.91*	− 0.15	− 0.14	*0.86*	0.24	*− 0.91*	*− 0.92*	*1*	
b^*	*− 0.88*	*0.87*	*0.89*	*0.93*	*0.7*	*0.89*	*0.92*	*0.88*	− 0.17	− 0.03	*0.79*	0.3	*− 0.87*	*− 0.88*	*0.97*	*1*

Values in italic are different from 0 with a significance level alpha = 0.05

of the bedrock. Likewise, the low levels of Al_2O_3, Fe_2O_3, K_2O, Na_2O, and SO_3 (less than 1% each) indicate the rarity of clays, sulfides, and sulfates. The sum of coloring oxides Fe_2O_3, TiO_2, Mn_2O_3, and Cr_2O_3 varied from one site to another without, however, exceeding 0.9%. High values coincided with fractures, karst corrosion, especially near bedding planes, and tectonic discontinuity.

The correlations table (Table 4) demonstrates a relatively high redundancy in the original data particularly between L^* and CaO (0.99), L^* and SiO_2 ($r = 0.99$), Al_2O_3 and TiO_2 ($r = 0.99$), Al_2O_3 and Na_2O ($r = 0.98$), SiO_2 and Al_2O_3 ($r = 0.99$), SiO_2 and TiO_2 ($r = 0.99$), SiO_2 and Fe_2O_3 ($r = 0.88$), and SiO_2 and CaO ($r = -0.91$), and thereby some of these variables can be removed without statistically significant influence on the quality of the interpretation.

The variability explained by the first two factors is relatively high (81.8%), ensuring that the map based on F1 and F2 factors has a good quality of projection of the initial data. P_2O_5, Cl, and MnO are closer to the center of the correlation circle (Fig. 3) and weakly correlated to the rest of variables ($|r| \leq 0.47$), which indicates that they play a non-significant role in the variability of the system. All other variables, however, fall close to perimeter of the correlation circle on F1 and

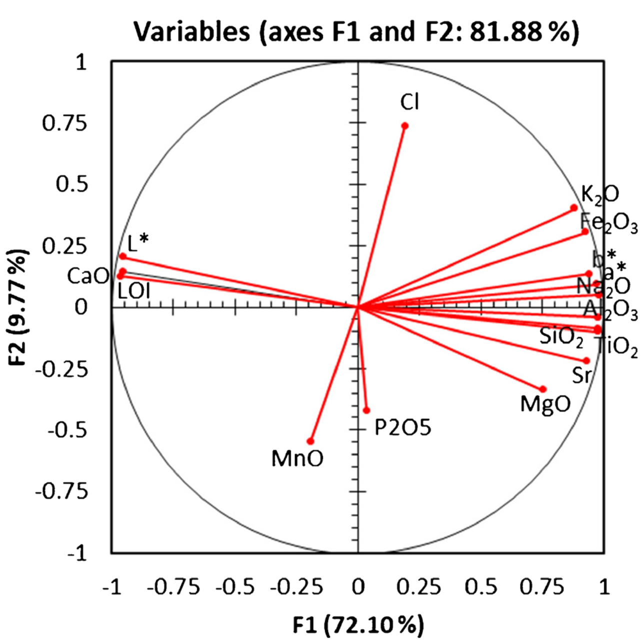

Fig. 3 Correlation circle based on F1 and F2 factors

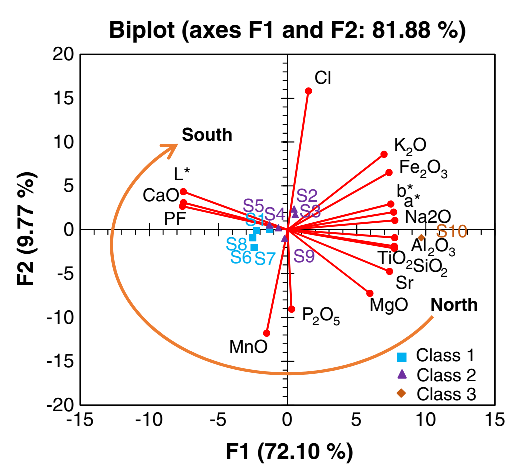

Fig. 4 Diagram of observations based on F1 and F2 factors

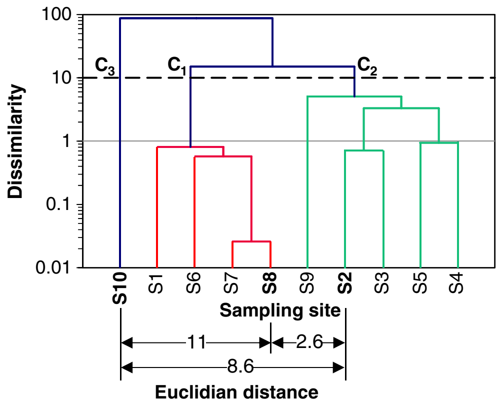

Fig. 5 Generic view of dendrogram-based Ward algorithm and Euclidian distance. In bold, nearest observation to the centroid of the group

F2 axes (Fig. 3). This position indicates that they are strongly correlated and it is possible to predict some of them based on other variables as can deduced from the correlation table (Table 3). *L**, CaO and LOI are close together and strongly correlated ($r \geq 0.98$), while they are negatively correlated to SiO_2, Fe_2O_3, Al_2O_3, Na_2O, K_2O, Sr, TiO_2, a* and b* stimulus ($r \leq -0.73$) found at the opposite perimeter of the circle (Fig. 3). The strong positive correlation $r \leq -0.74$ between (SiO_2, Al_2O_3, Fe_2O_3, MgO, K_2O, Na_2O) and (*L**, CaO) supposes that these elements derive from clay and weathering materials or diagenetic effects.

The brightness reading increases with the increase of the content of light minerals as calcite and decreases as the level of dark minerals, especially iron oxides and clay minerals, increase. These appear to be the primary factor responsible for color changes of the limestone. The red stimulus (*a**) is higher than zero for all considered samples, which supposes that iron oxide is the most common impurity that results in whiteness variations compared to manganese and titanium oxides. Likewise, the yellow stimulus (*b**) is higher than *a**, which suggests, theoretically, a light-yellow hue. Visually, the

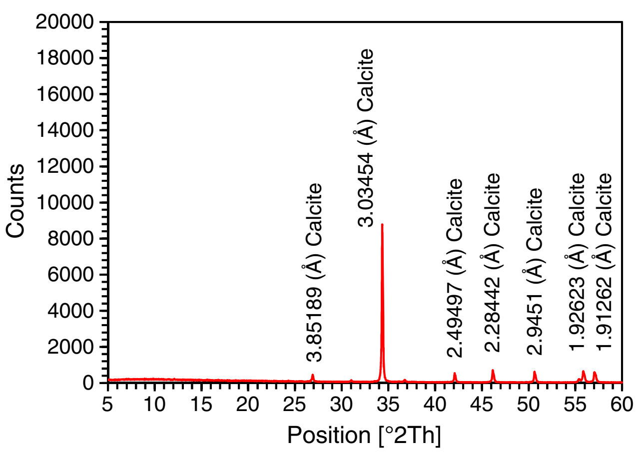

Fig. 6 XRPD specter showing the mineral composition of the BDG Member (Sidra site)

Table 5 Purity classification of GCC based on main harmful oxides MgO, SiO_2 and Fe_2O_3 values (Köhler et al. 2012)

	MgO (%)	SiO_2 (%)	Fe_2O_3 (%)	Acid insoluble (%)
Measured	< 0.4	0.7	0.4	< 0.1
Very high purity	< 0.8	< 0.2	< 0.05	
High purity	< 1	< 0.6	< 0.1	
Medium purity	< 3	< 1	< 1	
Low purity	> 3	< 2	> 1	

rock has light reddish hue due to hematite, which masks the yellow color from goethite (Fe_2O_3 and FeO(OH), respectively.

The diagram of observations on F1 and F2 factors (Fig. 4) shows that the limestone from Barre de Ghomrassene are subdivided into two main groups, which differ essentially in their whiteness including extra-white to white limestone (S1 to S9 sampling sites) and relatively dark-colored limestone in the north of the study area near el Farech (S10 sampling site).

The intrinsic grouping of sampling sites by classes or clusters of dissimilarity was performed using the hierarchical agglomerative clustering (HAC) method based on the Ward algorithm. Three groups of sampling sites were found (Fig. 5). Each class was represented by its central object, which are S8, S2, and S10. The representative sampling sites thus obtained were used to elaborate paint films. The difference in group number between PCA and HAC is due to the low Euclidian distance between the two first classes (2.6). These results indicate that the BDG limestone may exhibit significant lateral changes in relation to marine and continental interactions, surficial alteration, karstification, and diageneses (dolomitization), which may alter GCC quality. During exploitation, higher-grade parts should be separately extracted and adequately mixed with lower-grade parts in order to maximize economic benefits (Aloui and Chaabani 2008).

The mineral cortege of limestone beds (Fig. 6) is composed quasi-exclusively of calcite (3.034 Å). Most often, the percentages of calcite exhibit an upward increasing trend. Based on common values CaO and LOI, the calcite ranges from 97 to 98.7% (97.8% in average), which confirm the high

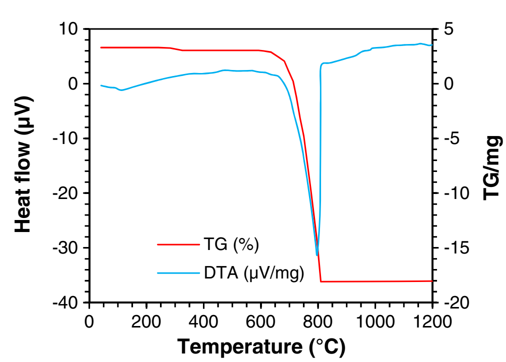

Fig. 7 DTA and TG of GCC from the Barre de Ghomrassene Member

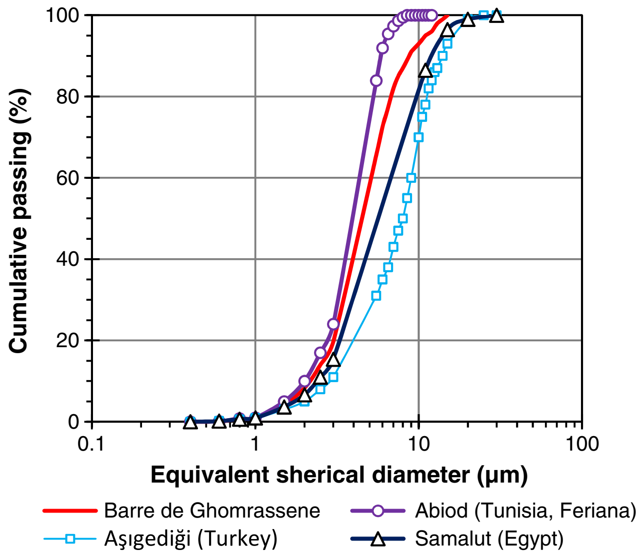

Fig. 8 Grain size distributions of representative ground calcium carbonates from Aşıgediği Formation* (Turkey), Abiod Formation (Tunisia, Feriana), Samalut Formation* (Egypt), and Barre de Ghomrassene Member. (*) data from provider

to very high grade of GCC as estimated through the Bernard calcimeter and semi-quantitative XRPD methods (≥ 97%).

The amounts of harmful compounds as MgO, SiO_2, and Fe_2O_3 oxides and acid insoluble (Table 5) are relatively low for all considered sites (less than 0.7% for each oxide and 0.1% for acid insoluble). This evaluates the deposit as of medium to very high purity.

Physical and mechanical properties of the Barre de Ghomrassene carbonate

The specific gravity of limestone from the Barre de Ghomrassene varies from 2.68 to 2.71 with an average of 2.7. The abrasion loss of limestone aggregates in the presence of water and an abrasive charge (micro-Deval test) are in general between 10 and 18 measured at upper part of the BDG from S5 site near Bir Thlathine and lower dolomite layers from S9 towards El Farech site respectively.

Thermal behavior

Through the thermogravimetric analysis depicted in Fig. 7, all tested samples exhibited a slight loss in weight by about 1% at 100 °C due to the evaporation of water from humidity or retaining residual attraction by adsorption on the surface of the sample. When temperature reached 800 °C, samples showed a sharp endothermic peak with a loss of about 55% of the weight due to the decomposition of lime according to the reaction $CaCO_3 \rightarrow CaO + CO_2$.

GCC grain size distribution

The GCC grain size displayed a Gaussian distribution with a spherical equivalent diameter ranging from 0.4 to 59.75 µm (Fig. 8). Particle size retained sieve 45 µm was most often less than 15% (2.2–4%) and the mean equivalent spherical diameter (D_{50}) was between 2.8 and 4.9 µm), which is in good agreement with required range for paint and coating (10–18 µm) (Köhler et al. 2012). The approximate sizes of finer particles (3th percentile) and coarser ones (97th percentile) of the GCC distribution were 0.59–0.63 and 10.4–36.2 µm, respectively.

The uniformity coefficient defined as Cu = D60/D10 of GCC ranged from 4.53 to 6.35 (5.27 in average). The curvature coefficient expressed as $Cc = D30^2/(D60.D10)$ varied between 0.76 and 3.14 (2 in average). These results indicate that the distribution was not regular in time and may be ranked as well-graded with wide size range (Cu > 6 and 1 < Cc < 3) to poorly graded (Cu ≤ 6). However, based on average values of uniformity and curvature coefficients, the distribution may be considered as poorly graded in which a narrow size range is dominant.

Under scanning electron microscopy (Fig. 9), the calcite particles were relatively uniform in terms of size and shape. Generally, this uniformity results in a consistent paint film formation on the surface which directly affects its appearance, coverage, opacity, gloss, and scrubbing resistance (Karakas et al. 2015).

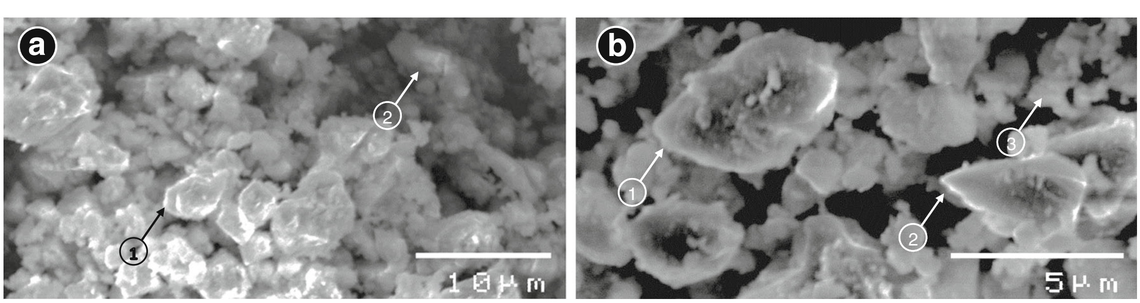

Fig. 9 SEM micrographs showing the morphology of the GCC from the Barre de Ghomrassene. **a** GCC with frequent sub-rounded and pellicular particles (1). **b** Closer view showing over ground carbonate calcite particles with frequent smooth edges and no sharp cleavage (1), rare angular grains (2), and fines (3)

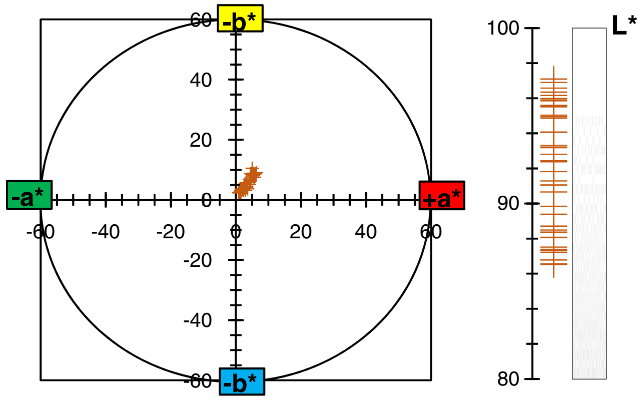

Fig. 10 Variations of L^*, a^*, and b^* stimulus for the GCC from the Barre de Ghomrassene Member

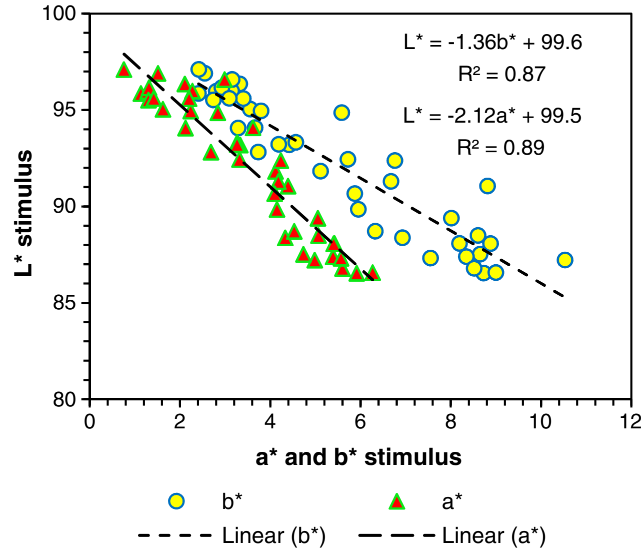

Fig. 12 Variations of L^* as function of a^* and b^* stimulus for the GCC from the Barre de Ghomrassene Member

Chromaticity

The lightness reading L^* of the limestones from the BDG Member were high and ranged from 86.53 to 97.1 with an average of 95.2 ($n = 42$, Fig. 10). The hue of the samples was dull and showed in overall a slight trend towards the yellow-red color ($a^* = 2.3$ and $b^* = 5.6$). Most often, L^* reading decreased from top to bottom layers and, to a lesser degree, from south to north. Near fault zones and karstic cavities (Fig. 11), the limestones become typically darker and reddish to yellowish in color.

To determine the cause of the color changes, Fe_2O_3 content was plotted against depth. The resulting profile seems to be symmetrical to whiteness with a correlation coefficient of 0.88 (Fig. 11). Therefore, the iron oxides are the primary factor that control the color changes of the limestones from the BDG. The red reading (a^*) is higher than zero for all samples, which ensures that compared to iron the other types of oxides have a secondary effect on the whiteness variation. The yellow reading (b^*) is consistently higher than a^* (Fig. 12), which suggests, theoretically, a light-yellow hue of the sediment. Visually, however, the limestones have a light reddish hue due to hematite (Fe_2O_3), which masks the yellow color from goethite (FeO(OH)). Elsewise, coarse and rounded bioclastic fragments, fossils debris, reef milk, and calcarenite are indicative of a shallow and relatively turbulent water environment such as reef talus or back reef. The brightness of sediments is in most often low and unsuited for paint and coating application. The lack of fine sand and silt across

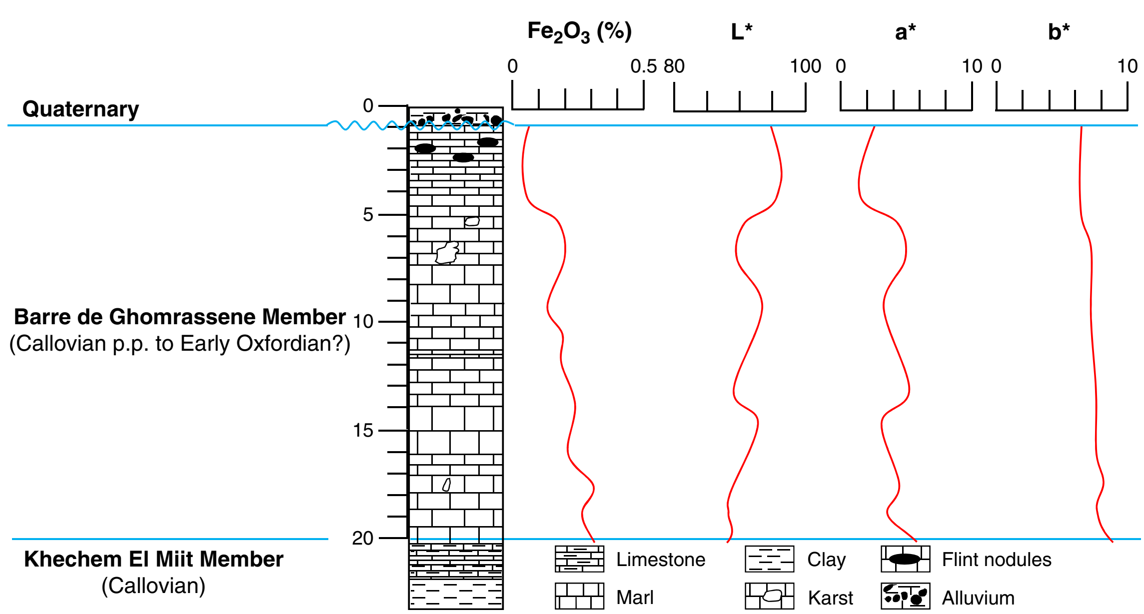

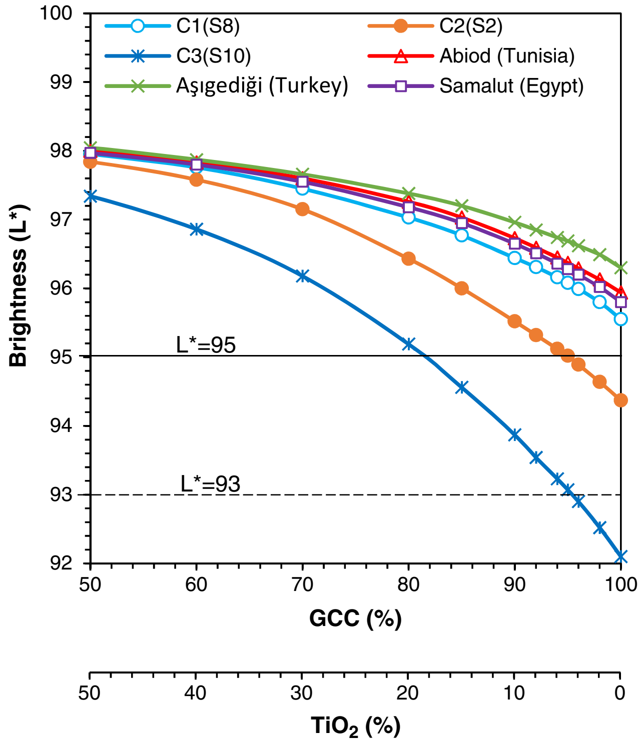

Fig. 13 Variations of brightness of tested GCCs as function of TiO_2. The solid line represents the optimum value of brightness. However, the dashed one represents the cut-off value of brightness, below which the quality of GCCs is considered too low to be used in paint

the lithostratigraphic column suggests that the deposition is not near the deep-water boundary.

Oil absorption

The oil absorption, or also oil number is in overall low to rarely ultra-low and varies between 14.5 and 22.7 ml/100 g GCC with an average of 17.4 ml/100 g GCC. This relatively low oil absorption is an advantage as it requires less vehicle to bind it, which eaves more vehicle available to bind to the substrate. The difference in the oil number may be attribute to the used method itself, which is very operator dependent (Köhler et al. 2012), the relative proportions of fine and coarse particles and grain shape, surface, and mean size. Higher oil numbers of GCC are indicative of very fine and regularly shaped calcite particles with higher specific surface, and hence more binder (resin) is required to bind them. Ultra-low oil numbers (less than 15 g/100 g GCC), however, are indicative of very coarse irregularly shaped calcite particles (Broad et al. 1993). These results confirm an adequate grinding of limestones.

Minimum quantity of pigment needed for $L^* = 95$

Brightness is the main quality parameter in the production of GCC used as filler in paint. Most often, raw materials should have a brightness greater than 93 and regular in time (Köhler 2012). To improve its brightness, croissant quantities of TiO_2

Table 6 Main characteristics of the GCC from the Barre de Ghomrassene Member compared to those from Abiod Formation (Tunisia, Feriana), Aşıgediği Formation (Turkey), and Samalut Formation (Egypt)

	BDG	Abiod	Aşıgediği	Samalut	Tolerance value[a]
CaO (%)	53.9–(54.5)–55.2	55.1–(55.3)–55.5	55.5	55.5	≥ 54.3
MgO (%)	0.2–(0.28)–0.37	≤ 0.2	< 0.3	< 0.08	≤ 1
Acid insoluble (%)	≤ 0.1	≤ 0.1	< 0.1	< 0.1	≤ 2
Density	2.65–2.71	2.6–2.7	2.7	2.7	2.7
Oil number (g/100 GCC)	14.6–(17.4)–22.7	14.7–(17.1)–18.5	15.6–(18)–21.1	15–(18)–21	10–(18)–20
Lightness (L^*)	86.5–(95.2)–97.1	86–(95.8)–97	96.1	95.7	75–95
Red-green reading (a^*)	0.8–(2.3)–3.3	0.9–(1.4)–1.9	2.1	2.7	–
Yellow-blue reading (b^*)	2.4–(5.6)–9.1	2.7–(5.4)–8.4	5.2	5.9	–
Blaine surface (cm^2/g)	3000 ± 200	3000 ± 200	3000 ± 200	3000 ± 200	500–3000
pH	9	9	9	8.9	9 ± 0.5
Particle size range (μm)	0.4–45	0.4–70	0.5–70	1.2–100	0.5–100
Mean grain size (μm)	2.8–(4.1)–4.9	0.9–(4)–13	1.1–(7.8)–15.2	1.9–(5.2)–10	6
Passant on 45 μm (%)	100	95.2–(97.6)–100	98.2–100	94.5–100	100
Passant on 30 μm (%)	96.3–(98.7)–100	84.7–(92.6)–100	87–100	86.3–100	99.8
Passant on 20 μm (%)	88.2–(95.1)–99.9	70.3–(86.8)–100	66.4–100	74–100	97
Passant on 10 μm (%)	70.3–(79.9)–89.5	45.5–(70.1)–100	31–100	50–100	75
Passant on 3 μm (%)	38.1–(46.5)–53.1	23–(50.7)–70.6	10.5–96.4	19–67.7	50
Abrasion	10–18	–	–	–	–
Hardness-Mohs	3–4[a]	3–4[b]	3	3	3

[a] Köhler et al. 2012

[b] For dolomitic limestone strata

[c] For sandy limestone strata. Mean values are in parenthesis

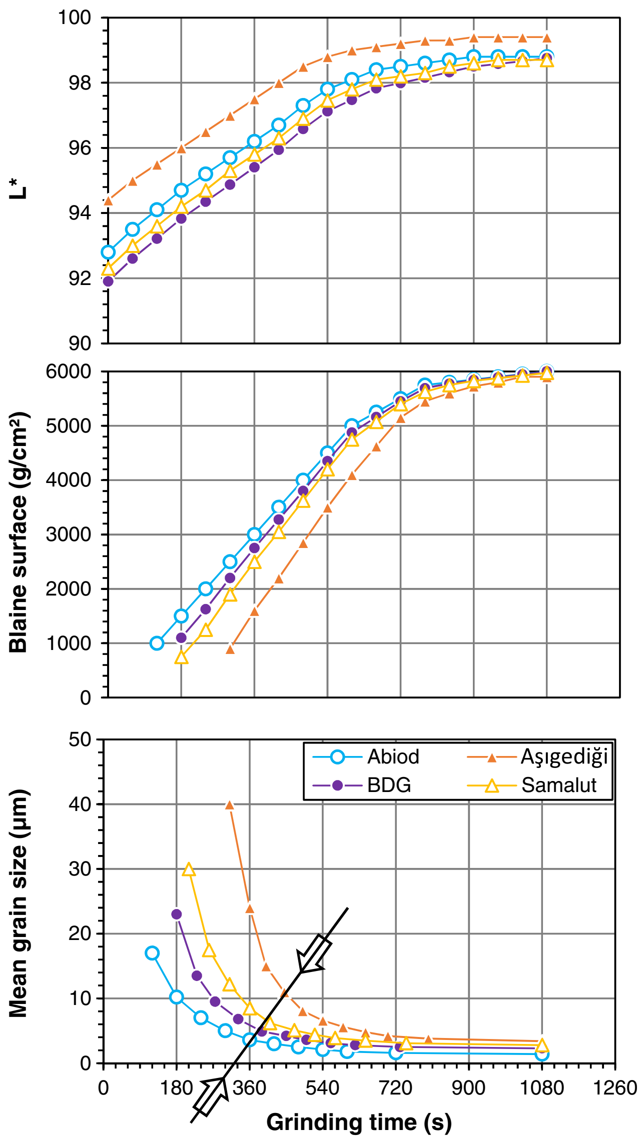

Fig. 14 Effects of grinding time on mean particle size, Blaine specific surface and brightness of GCCs from the BDG Member, the Abiod Formation, the Samalut Formation, and the Aşıgediği Formation. The arrows indicate the inflection point for each tested GCC

were added to GCC (Fig. 13). The results indicate that the substitution of GCC by TiO_2 shifts significantly the brightness of the mixture. GCCs from S2, S8, Samalut, and Abiod formations require low values of TiO_2 to get a brightness of 95 in particular for S2 site (greater than 5% TiO_2). While S10 sample site, near the El Farech, needed mush higher TiO_2 (greater than 18%) as can be seen in Fig. 13. This increase in brightness exhibits a non-linear trend due to the fact that luminescence values are not additive (Järnström et al. 2008; Couper et al. 2012). Likewise, the brightness curves are smooth elsewhere because we used the same sample of GCC, which reduce the effects of particle size distribution, grain morphology, hardness, elasticity, roughness, and cleavage on its optical properties. It is evident that the GCC sourced from S10 sampling site is not suitable for paint industry since it has a low brightness ($L^* = 93$) even after adding 5% of TiO_2 and high MgO concentration (3.8%).

Comparison of the GCC from the Barre de Ghomrassene with Mediterranean GCCs

The GCC from the BDG meets all the requirements of paint production including purity, acid insoluble, density, oil number, lightness, grain size mean and distribution, pH, and hardness-Mohs (Table 6). In comparison with nearby GCC, the studied GCC explains slightly less lime (55.1% CaO) compared to those from Aşıgediği and Samalut formations (55.5% each) and Feriana Mountain (55.3%).

The mean oil number is close to tolerance value (18 g/100 g GCC in average) for all considered samples and ranged from 14.6 to 22.7 g/100 g BCC. For Tunisian GCCs, however, it is slightly lower (17.1–17.4 g/100 g GCC in average). This difference may be attributed to the fact that graded GCCs are able to be compacted more than poorly graded ones, which leads to a less available space for binder.

The grinding stage of GCC materials is an increasingly important process in coating and painting industries. Indeed, the reduction of particle size is very expensive and the energy requirements as well as cost per tonne of filler. Specific surface of GCC is one of the most critical of its physical properties, because it controls the appearance of the end product and promotes rapid chemical reactions, through the exposure of large surface areas to reactants (binder and additives). Hence, the time to achieve the desired specific surface and brightness is a key parameter during the grinding process.

The increase in the grinding time results in the particle size distributions moving towards the finer sizes, which shifts the Blaine surface by approximately 500 to 600 $g/cm^2/min$ of grinding during the first 10 min for all considered GCCs (Fig. 14). The influence of increased milling time on the particle size distribution is relatively higher for non-metamorphic carbonate. At 10 min of continuous grinding, the Blaine surface ranges from 4000 to 5000 g/cm^2 respectively for Aşıgediği Formation and Abiod Formation. For longer grinding times, the Blaine surface values become close to each other and remains quasi-unchanged at about 5500 g/cm^2.

The grindability test shows that limestones from the BDG Member, the Abiod Formation, and to a lesser degree the Samalut Formation need a grinding period of about 6 to 7 min to achieve a mean particle size lower than 6.2 µm, a Blaine fineness of 3000 ± 200 m^2/g GCC, and a brightness greater than 95. The Aşıgediği Formation, however, needs much more time (1 to 2 mn later). This may be attributable to the strength of calcite particles, which increases with the degree of metamorphism. The small difference in grindability between non-metamorphic GCCs may be attributable to

Table 7 Main characteristics of painted films based GCC from the Barre de Ghomrassene Member compared to those from Abiod Formation (Tunisia, Feriana), Aşıgediği Formation (Turkey), and Samalut Formation (Egypt)

Parameter	Value/appreciation					
	S1	S2	Abiod	Aşıgediği	Samalut	Typical[a]
Surface dry (h)	1–2	1–2	1–2	1–2	1–2.5	
Through dry (h)	3–4	3–4	3–4.5	3–4	3–5	
Dry film thickness (μm)	112	118	123	106	131	
Brightness (L^*)	96.6	95.8	96.7	97.4	96.5	
Opacity	Very good	Very good	Very good	Very good	Very good	Very good
Visual gloss[b]	Matt	Matt	Matt	Matt	Matt	Matt
Color	White	White	White	White	White	White
Hardness (s)[c]	145	142	140	144	148	
Adhesion by cross-hatch	smooth edges (B5)	B5, rare small flacks (B4)	B5	B5	B5, rare B4	B5–B4
Impact resistance (kg m)	1.5	1.5	1.5	1.4	1.4	

[a] Three local commercial water borne paints

[b] Dualgloss 20/60°

[c] By pendulum damping test

chemical diagenesis effects. These results the good grindability of non-metamorphic limestones.

The increase in grinding time contributed to shift L^* values by 0.4 per minute in average for all considered GCCs. The difference between feed values and end values may reach 5 to 6–6.8 for metamorphic carbonate (Aşıgediği Formation) and non-metamorphic carbonates (BDG Member, Samalut Formation, and Abiod Formation). The value of a^* (red-green reading) decreased by 2 after a grinding time of 10 min, while b^* (yellow-blue reading), decreased by 1 in average, for the same period of grinding time. These results reveal the importance of grinding to improve the appearance of tested GCCs. The decreasing in the theoretical mean diameter (Q_{50}) contributes to scattering light by altering the spatial distribution of the pigments in the dry film (Gündüz 2015).

Physical and mechanical properties of paints

The main characteristics of formulated emulsions include pH and viscosity. A decrease in pH can affect largely the end product performance and conformance. The pH values were high and close to optimal value (9) for all considered of emulsions (Köhler et al. 2012). This range of pH stabilizes additives in the emulsion, resulting in a film with good adhesion and appearance in term of color and texture, and high gloss (Dillon et al. 2014). The majority of paints, mainly architectural paints, include all the necessary nutrients (organic matter) and water for growth of both aerobic and anaerobic microorganisms if the pH is in the range of 5 to 7. Since most used biocides destroy at a pH greater than 9.5 (Lindner 2001), a pH closer to 9 will inhibit the proliferation of these microorganisms, while keeping the biocides active, which gives a good and regular smell to the painted film.

To ensure proper functionality of the thickener, the acidic groups in the polymer chains should be neutralized by shifting the pH value between 8 and 9.5. While, the reaction of polymerization of binder to form a cohesive film requires basic media with a pH range of 7.5–8.5. Hence, a final pH of 9 ensures an optimum thickening and maintains a stable viscosity of paint.

The viscosity of paints is in the range of 91–113 Krebs unit (KU) for all tested samples with an average of 97 KU, and is in concordance with bibliographic values for GCC extender (80–120 KU) (Köhler et al. 2012). These slightly higher levels of viscosity may be due to the decrease in grainsize of GCC particles during either the initial grinding of limestone or the paint preparation.

Physical and mechanical properties of the painted films

Results of physical and mechanical tests applied to the elaborated films are reported in Table 7. In general, the surface of painted films takes 1 to 2 h to dry and no longer adheres to the finger when pressed firmly or rubs up when rubbed lightly. After drying, the painted films are in general 85–140 μm thick (Fig. 15) and display a matt surface without any significant tint or haze (PVC = 82.7%). Also, they furnish good opacity, appearance, and visibility under both daylight and artificial light. This ensures that the tested films were overcured and good adhesion to the substrate (Hansen et al. 1994). Hardness values of cured films are in general suitable and range between 120 and 140 s. The impact resistance values grade from 1.4 to

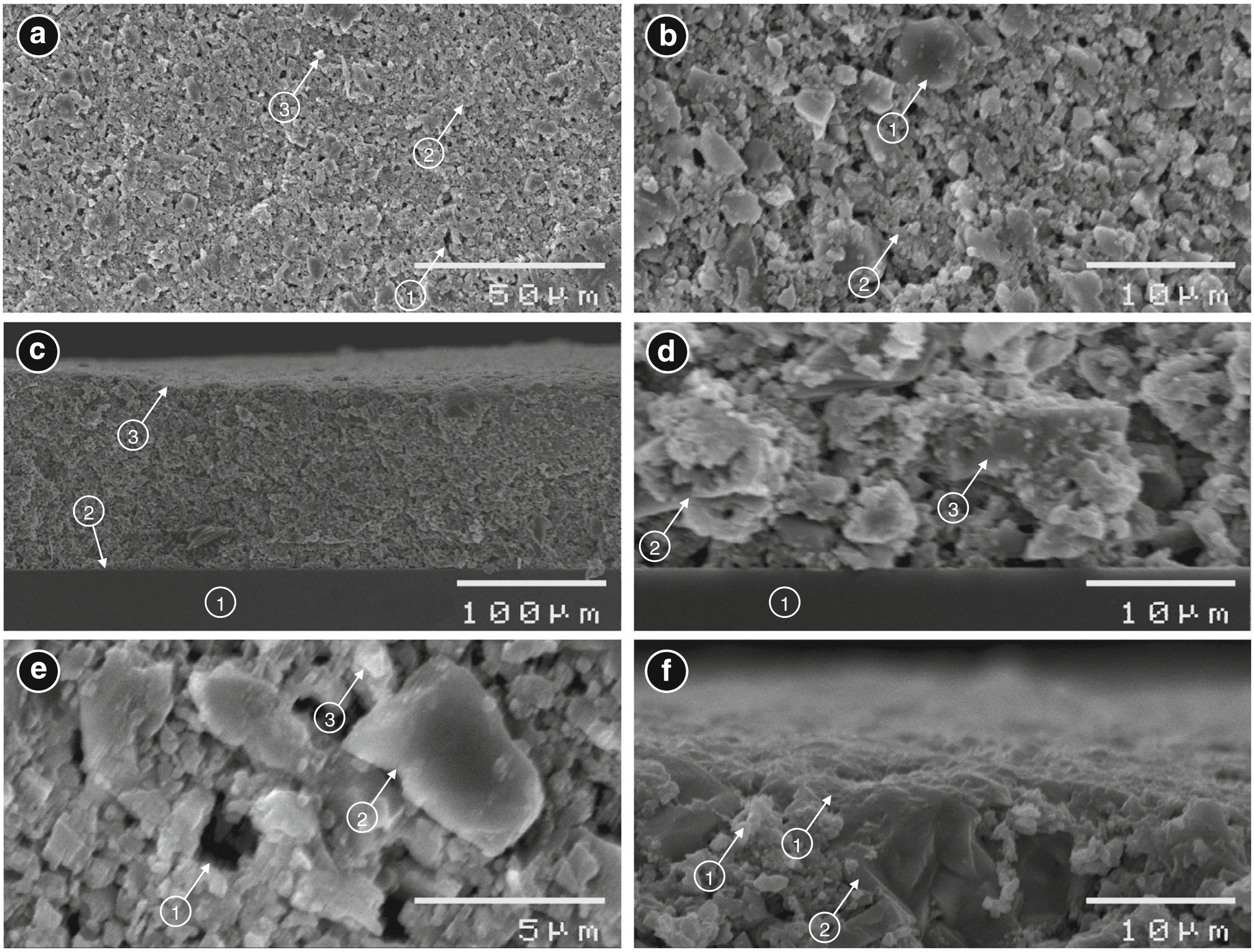

Fig. 15 SEM micrographs of a dry paint film showing the ultrastructure of the film. **a** Top view showing smooth and matt surface of film with rare pores of volatiles (1), polymer matrices (2), and white particles of titania (3), used due to its high refractive index. **b** Closer view of micrograph (**a**) showing a sub-rounded calcite particle (1), which floats on the polymer matrices (2). **c** Section showing a relatively regular thickness of the paint film, which coats the substrate (1). (2) and (3) refer to lower and upper surfaces of the film. No vertical stratification trend is visible. **d** Closer view of the lower surface of the paint film of the micrograph (**c**). (1) substrate, (2) polymer matrices, and (3) angular calcite particle. **e** Closer view of the top surface of the paint film of the micrograph (**c**), showing a small pore of volatiles (1), rectangular calcite particle with sharp edges (2), and white area of titania (3). **f** The upper most part of the micrograph (**a**), which displays a smooth and continue layer of the polymer matrices (1) that coat titania (2), and calcite (3) particles. This may improve coverage capability, washability, and appearance effects of the paint film

1.6 kg m, which indicates good coating of test films. After application of the adhesion test, the edges of the cuts appeared to be smooth for major part of considered films (class 5B). However, sparse small flakes of the coating are detached at intersections (class B4).

Conclusions

In the light of the above results and discussions, the following conclusions could be highlighted:

1- The limestone from the Barre de Ghomrassene between Ksar Ouled Dabbeb and Bir Thalathine are characterized by a high to very high degree of purity, which grades from 94.5 to 98.6% calcite (97.1% on average). The content on harmful elements such as MgO (less than 0.4% on average), Al_2O_3, Fe_2O_3, K_2O, Na_2O, and SO_3 (less than 1% each) is low. Likewise, the sum of coloring oxides Fe_2O_3, Mn_2O_3, and Cr_2O_3 may be detectible near fractures, karst corrosion, bedding planes, and tectonic discontinuity, but do not exceed 0.9%.

2- The limestone is bright white with ($L^* \geq 86.5$, 95.2 in average), with a slight trend towards yellow-red hue ($a^* = 2.3$ and $b^* = 5.6$). The brightness (L^*) increases as light minerals like calcite and quartz increase and decreases with increase in coloring oxides especially iron oxide. In general, it increases from bottom to top layers and, to a lesser degree, from north to south. Near fault zones and karstic cavities, the limestone becomes darker and reddish to yellowish in color.

3- The ground calcium carbonate (GCC) of the study area has a low oil intake (17.4 g/100 GCC), very low acid insoluble residue (less than 0.1%), easy dispersion, very low electrolyte levels, pH buffering (close to 9), and improved rheological properties.

4- The painted films formulated based on GCC from the Barre de Ghomrassene using a standard recipe meet all requirements, with suitable hardness, good adhesion, high impact resistance, very good opacity, matt visual gloss, and high luminescence reading greater than 93.

5- The performances of painted films are analogous to those based on natural carbonates (Abiod and Samalut formations), but they are slightly less lighter than those based on metamorphic carbonates (Aşıgediği Formation).

6- The studied GCC can be used to substitute them in particular for local GCCs from the Abiod Formation, which are limited and over exploited.

References

Aas E (1996) Refractive index of phytoplankton derived from its metabolite composition. J Plankton Res 18(12):2223–2249

Allen T (1990) Particle size, shape and distribution. In: Allen T (ed) Particle size measurement. Springer, pp 124–191. https://doi.org/10.1007/978-94-009-0417-0_4

Aloui T, Chaabani F (2006) Influence of fractures and karstification on the development of a quarry at Jebel Feriana, Tunisia. Bull Eng Geol Environ:345–351

Aloui T, Chaabani F (2007) Influence of fractures and karstification on the development of a quarry at Jebel Feriana, Tunisia. Bull Eng Geol Environ 66:345–351. https://doi.org/10.1007/s10064-006-0073-y

Aloui T, Chaabani F (2008) Maastritchian limestones of Feriana Mountain used in white cement production (Central West Tunisia). J Am Ceram Soc 91(11):3704–3713

Aloui T, Dasgupta P, Chaabani F (2012) Facies pattern of the Sidi Aïch Formation: Reconstruction of Barremian paleogeography of Central North Africa. Journal of African Earth Sciences 71:18–42. https://doi.org/10.1016/j.jafrearsci.2012.06.004

Aloui T, Ounis A, Dasgupta P, Lourimi W, Chaabani F (2017) Depositional history of the Late Barremian deposits (Sidi Aïch Formation) in central Tunisia and adjacent parts of Algeria: A geostatistical revelation. J Afr Earth Sci. https://doi.org/10.1016/j.jafrearsci.2017.11.037

Ariffin KS (2003) Prediction of energy consumption of geologically different marble deposits in ground calcium carbonate (GCC) production. Geological Society of Malaysia Bulletin 46:255–262

ASTM (2008) Standard test method for specular gloss. Designation: D523–89. American Society for Testing and Materials, USA. https://doi.org/10.1520/D0523-89R08

ASTM (2010) Standard test method for resistance of organic coatings to the effects of rapid deformation (impact). Designation: D2794. American Society for Testing and Materials, USA. https://doi.org/10.1520/D2794-93R10

ASTM (2013) Standard test methods for measurement of wet film thickness of organic coatings. Designation: D1212–91. American Society for Testing and Materials, USA. https://doi.org/10.1520/D1212

ASTM (2014a) Standard test methods for specific gravity of soil solids by water pycnometer. Designation: D854–14. American Society for Testing and Materials, USA. https://doi.org/10.1520/D0854-14

ASTM (2014b) Standard test method for consistency of paints measuring Krebs unit (KU) viscosity using a Stormer-type viscometer. Designation: D562–10. American Society for Testing and Materials, USA. https://doi.org/10.1520/D0562-10R14

ASTM (2016) Standard test method for oil absorption of pigments by spatula rub-out. Designation: D281–12. American Society for Testing and Materials, USA. https://doi.org/10.1520/D0281-12R16

ASTM (2017a) Standard test method for resistance of coarse aggregate to degradation by abrasion in the micro-deval apparatus. Designation: D6928–17. American Society for Testing and Materials, USA. https://doi.org/10.1520/D6928-17

ASTM (2017b) Standard test methods for rating adhesion by tape test. Designation: D3359–17. American Society for Testing and Materials. https://doi.org/10.1520/D3359-17

Ben Ismail, MH, Razgallah SG, Cuif JP, Gautret P (1989) Découverte de biohermes à Démosponges calcifiées dans le Callovien supérieur du sud tunisien.Implications paléobiologiques et sédimentologiques. Géol Méditerr XVI, 2-3:201–211

Bentz DP, Garboczi EJ, CHaecker CJ, Jensen OM (1999) Effects of cement particle size distribution on performance properties of Portland cement-based materials. Cem Concr Res 29(10):1663–1671. https://doi.org/10.1016/S0008-8846(99)00163-5

Bishay Y (1961) Biostratigraphic study of the Eocene in the Eastern Desert Between Samalut and Assiut by the larger Foraminifera. 3rd Arab Petroleum Congress, Alexandria, Paper n° 13 (B-3)

Bishay Y (1966). Studies on the larger foraminifera of the Eocene (the Nile Valley between Assiut and Cairo and SW Sinai). PhD. thesis, Alexandria University

Blanco-Varela MT, Palomo A, Puertas F, Vazquez T (1997) CaF2 and CaSO4 in white cement clinker production. Cem Concr Res 9(35): 105–113

Broad R, Power G, Sonego A (1993) Extender pigments. In: Oil and Colour Chemists' Association (ed) Surface coatings, Springer, pp 514–529. https://doi.org/10.1007/978-94-011-1220-8_29

Busson G (1967) Le Mésozoïque saharien. 1ère partie : l'Extrême Sud tunisien. – C.N.R.S. Edit., Paris, « Centre Rech. Zones arides ». Géol 8:194

Chaudhury M, Pocius AV (2002) Adhesion science and engineering: surfaces, chemistry and applications. 1st ed. 2014p. ISBN-13: 978-0444511409

CIE (Commission Internationale de l'Eclairage) (1986) Standard on colorimetric observers. CIE S002, New York

Conley RF (1983) Attrition milling of industrial minerals. In: Malghan SG (ed) Proceedings ultrafine grinding and separation of industrial minerals, SME-AIME, New York, pp 37–48

Couper JR, Penney WR, Fair JR, Walas SM (2012) Chemical process equipment, 3rd edn. Botterworth-Heinemann (Elsevier), Oxford, 864 p

Cox F, Bridge, D McC, Hull JH (1977) Procedures for the assessment of limestone resources. Mineral Assessment Report N° 30. Institute of Geological Sciences, London, 16 p. https://www.bgs.ac.uk/downloads/start.cfm?id=2743. Accessed 26 Oct 2017

Dillon CE, Lagalante AF, Wolbers RC (2014) Acrylic emulsion paint films: the effect of solution pH, conductivity, and ionic strength on film swelling and surfactant removal. Stud Conserv 59(1):52–62. https://doi.org/10.1179/2047058412Y.0000000076

Enay R, El Asmi K, Soussi M, Mangold C, Hantzpergue P (2002) Un Pachyerymnoceras arabique dans le Callovien supérieur du Dahar (Sud tunisien), nouvel élément de datation du membre Ghomrassène (formationTataouine); corrélations avec l'Arabie Saoudite et le Moyen-Orient. C R Geosci 334:1157–1167

Eswaraiah C, Venkat N, Mishra BK, Holmes R (2015) A comparative study on a vertical stirred mill agitator design for fine grinding. Sep Sci Technol 50(17):2639–2648. https://doi.org/10.1080/01496395.2015.1065888

Göncüoğlu MC (1977) Geologie des westlichen Niğde Massivs: Bonn Univ., Ph.D. Thesis 181 p. (Unpublished)

Gündüz G (2015) Chemistry, materials, and properties of surface coatings. Traditional and evolving technologies. 751 p. ISBN-13: 978–1605950662

Hansen EF, Walston S, Bishop MH (1994) Matte paint: its history and technology, analysis, properties, and treatment, with special emphasis on ethnographic objects. Getty Conservation Institute. ISBN 0-89236-262-6. Retrieved 2015–03-11

International Organization for Standardization (2006) ISO 1522: paints and varnishes—pendulum damping test

Järnström J, Ihalainen P, Backfolk K, Peltonen J (2008) Roughness of pigment coatings and its influence on gloss. Appl Surf Sci 254: 5741–5749

Karakaş F, Celik MS (2012) Effect of quantity and size distribution of calcite filler on the quality of water borne paints. Prog Org Coat 74(3):555–563. https://doi.org/10.1016/j.porgcoat.2012.02.002

Karakas F, Hassas BV, Celik MS (2015) Effect of precipitated calcium carbonate additions on waterborne paints at different pigment volume concentrations. Prog Org Coat 83:64–70. https://doi.org/10.13140/2.1.3233.6325

Klieger P (1994) Significance of tests and properties of concrete and concrete-making materials, issue 169, part 3. Front cover. Paul Klieger. ASTM, 1994–. 639 p. ISSN 0066-0558. ISBN 0803120532, 9780803120532

Köhler K, Simmendinger P, Roelle W, Scholz W, Valet A, Slongo M (2012) Paints and coatings, 4. Pigments, extenders, and additives. Ullmann's encyclopedia of industrial chemistry. 22 p. https://doi.org/10.1002/14356007.o18_o03

Koleske JV (2012) Paint and coating testing manual, 15th edition of the Gardner-Sward handbook. ASTM International. ISBN 978-0-8031-7017-9

Lindner W (2001) New developments for in-can preservation of water-based paints and printing inks. Surface Coatings International Part B: Coatings Transactions 84(2):141–146. https://doi.org/10.1007/BF02699776

M'Rabet A (1987) Stratigraphie, sédimentation et diagenèse carbonatée des séries du Crétacé Inférieur de Tunisie Centrale. Ann Min Géol Tunis 30:410

Pohl WL (2011) Principles and practice metals, minerals, coal and hydrocarbons—introduction to formation and sustainable exploitation of mineral deposits. Wiley-Blackwell, Oxford, 699p. https://doi.org/10.1002/9781444394870

Ruste J (1978) Spectroscopie de rayons X (X-ray spectroscopy), Chap. 5, pp 219–272. Microanalyse–Microscopie Electronique A Balayage (Microanalysis–electron scanning microscopy), Edited by Les éditions de physique, France

Sdiri A, Bouazir S (2014) Re-evaluation of several heavy metals removal by natural limestones. Front Chem Sci Eng 8(4):418–432. https://doi.org/10.1007/s11705-014-1455-5

Somasundaran P (1978) Theories of grinding. In: Onoda G Jr, Hench L (eds) Ceramic processing before firing, 1st edn. Wiley, New York, pp 105–123

Whitney DL, Dilek Y (1998) Metamorphism during crustal thickening and extension in central Anatolia: the Nigde metamorphic core complex. J Petrol 39:1385–1403

Whitney DL, Teyssier C, Fayon AK, Hamilton MA, Heizler M (2003) Tectonic controls on metamorphism, partial melting, and intrusion: timing of regional metamorphism and magmatism of the Nigde Massif, Turkey. Tectonophysics 376:37–60